Numerical investigation of vibratory response of planetary gear sets and modulation effects induced by carrier rotation

Jessica Neufond, Joël Perret-Liaudet, Emmanuel Rigaud, Pascal - Bouvet, Adrien Parpinel

25-29 August 2024
inter.noise
NANTES FRANCE

Numerical investigation of vibratory response of planetary gear sets and modulation effects induced by carrier rotation

Jessica NEUFOND[1]
Vibratec
28 chemin du Petit Bois, 69130 ECULLY, FRANCE

Joël PERRET-LIAUDET[2]
Univ Lyon, ENTPE, Ecole Centrale de Lyon, CNRS, LTDS, UMR5513
36 Avenue Guy de Collongue, F69134 ECULLY cedex, France

Emmanuel RIGAUD[3]
Univ Lyon, ENTPE, Ecole Centrale de Lyon, CNRS, LTDS, UMR5513
36 Avenue Guy de Collongue, F69134 ECULLY cedex, France

Pascal BOUVET[4]
Vibratec

Adrien PARPINEL[5]
Vibratec

ABSTRACT

In geared systems, the main source of excitation is generated by the mesh process itself. Depending on the dynamic conditions involved, the system may present a variety of problems, ranging from acoustic nuisance to system failure. Predicting and controlling the mesh process at an early design stage is a key point to avoiding such issues. The problem is complex, mainly due to its multi-scale nature. Indeed, the vibroacoustic behavior of geared systems (on the scale of a meter) depends on the local micro-geometry of the teeth (on the scale of a micron), associated with the transmission error. Moreover, the problem is parametric in nature, due to the periodic fluctuation of the mesh stiffness. These parametric internal excitations generate dynamic mesh forces which are transmitted to the housing through wheel bodies, shafts and bearings. In the case of planetary gear sets, the numerical prediction presents a complementary challenge as, in many applications, the carrier rotation modulates the housing vibration response at its rotational frequency. This paper presents an original simulation process to deal with modulation effects in planetary gear systems.

1. INTRODUCTION

Among all the services offered by gear transmission systems, the level of noise pollution and service life are important items in the specifications. The impact of noise and vibration extends beyond technical considerations and has socio-economic implications. Noise pollution affects

[1] jessica.neufond@vibratec.fr
[2] joel.perret-liaudet@ec-lyon.fr
[3] emmanuel.rigaud@ec-lyon.fr
[4] pascal.bouvet@vibratec.fr
[5] adrien.parpinel@vibratec.fr

the well-being of citizens, while excessive vibrations can compromise the safety and performance of equipment and hardware. The costs associated with implementing measures to improve noise, vibration, and harshness (NVH) can also impact industry. In the past decade, the demand for silent gears has prompted engineers to adapt their models and incorporate novel solutions in transmission systems.

Driven gears under load create the whining noise. This acoustic behavior at different operating modes originates from time-varying excitation mechanisms such as eccentricity, manufacturing errors (profile and lead geometry), and assembly errors (parallelism and deflection). These excitations correspond to the Transmission Error (TE) and the instantaneous mesh stiffness fluctuations at a given applied torque. Dynamic mesh forces create structure-borne noise propagating from gear teeth to the housing via gearbox components (gears, shafts, and bearings) and radiates as audible airborne noise [1, 2]. One of the special features of geared systems is the multi-scale nature of the problem. Indeed, the overall dynamic and vibroacoustic behavior of the transmission (on the scale of a meter) depends on the local micro-geometry of the teeth (on the scale of a micron).

While the know-how developed has been applied to many fixed-axis gear applications, such as automotive gearboxes, the characterization of the overall behavior of multi-gear systems with moving axes, such as planetary gears, requires further research. Planetary gear sets are distinguished by their capacity to provide high gear ratios in a compact package. However, whining noise prediction and control remains a difficult problem because of the coupling between the multiple gear meshes and the relative mobility of the planet axes with respect to the ring gear, whatever the operating configuration. This mobility is at the origin of phenomena such as the modulation of the signal measured at a fixed point of the ring gear [5, 6]. The architecture of a single stage planetary gear is illustrated Figure 1.

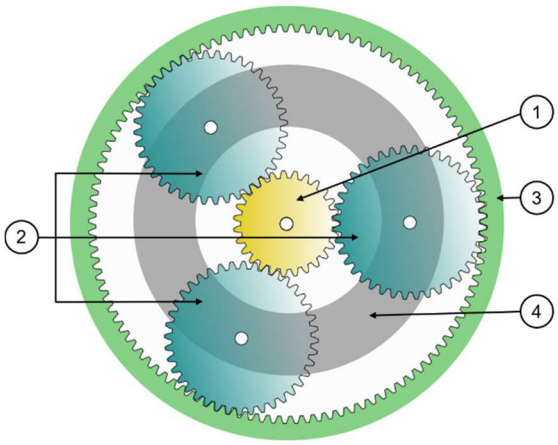

Figure 1: Planetary gear architecture. (1): Sun gear - (2) Planet gears - (3) Ring gear - (4) planet carrier

The iterative spectral method allows the solving of linear parametric equations of motion, in the carrier reference frame, in the spectral domain, with short computational time [7, 8]. The dynamic response at meshes is hence fully characterized and the short computational time allows parametric investigation. However, the computation of the dynamic response of any fixed point on the ring gear requires an additional step. Even if many works deal with ring gear modulated dynamic response [9-11], further work is required to include the ring gear's modal behavior contribution. Indeed, the existing methods propose a simplified formulation based on the use of Hanning window functions to simulate the growth/decay of the vibratory amplitude as one planet approaches or moves away from the measured fixed point. Though these

approaches give good correlation with experiments at low frequencies, the coincidence between mesh frequencies and housing modes at higher frequencies is less discussed.

Thus, this paper proposes a modal approach by considering the modulation effects induced by the relative rotation between the observation point (fixed point located on the ring gear) and the meshes (attached to the carrier reference frame).

2. STUDIED PLANETARY GEAR SET

The studied planetary gear set features the sun as its input and the carrier as the output. As a result, the ring gear remains fixed. Main characteristics are given in Table 1.

Table 1: Main characteristics of the studied planetary gear set.

	Sun	**Planets**	**Ring**
Number of planets N		3	
Number of teeth Z	27	40	108
Module m_0 (mm)		1.5	
Pressure angle α (°)		20	
Helix angle β (°)		0	
Ratio i_{sc}		5	

Based on the gear module, the maximum permissible input torque is 156 Nm, i.e. a breaking torque of 780 Nm. The nominal input operating speed of the planetary gear is 1500 rpm, with a maximum value of 3500 rpm. For experimental validation with a numerical model, the planetary gear is mounted on a test bench, as shown in Figure 2. Motors and planetary gear are connected by mechanical couplings.

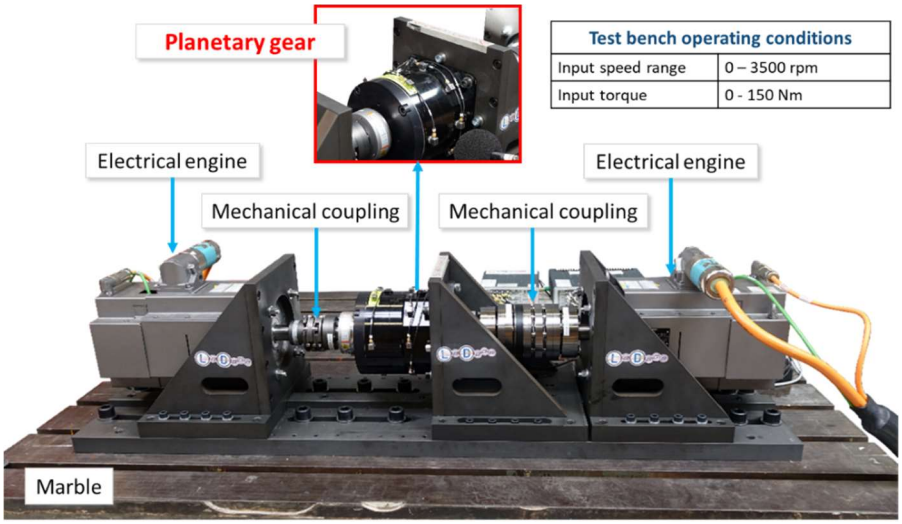

Figure 2: Planetary gear test bench.

3. NUMERICAL MODEL

The numerical process to access housing dynamic response can be divided into three main steps, summarized in Figure 2:

- Computation of static transmission error and mesh stiffness fluctuation at each mesh through the solving of contact equations,

- Computation of the dynamic response of the drive train through an iterative spectral method,
- Computation of the dynamic response of the housing through the relative rotation between the observation point (fixed point located on the housing) and the meshes (attached to the carrier rotating reference frame).

3.1 Static transmission error and mesh stiffness fluctuation

Assuming infinitely rigid and geometrically perfect gears, their circular involute profile offers a constant instantaneous transmission ratio. However, these undeformable and geometrical assumptions are never met. Geometrical errors of tooth correction as well as deformation under torque induce a fluctuation of the instantaneous transmission ratio around its theoretical value. This fluctuation results in the so-called Static Transmission Error (STE). It is defined as the deviation between the actual position of the output shaft and its theoretical position [1, 2]. STE calculation relies on the resolution of the static teeth contact equations. For each position θ of the driving gear, a kinematical analysis of the mesh allows the determination of the theoretical contact line on the tooth surfaces. Contact equation solving leads to STE δ(θ) evaluation and load distribution P over the contact lines.

In the case of planetary gears, equations of contact are solved taking account of all meshings *j* simultaneously. Unlike cylindrical gears with fixed axes, the input torque is not necessary shared equally between the planet gears. Thus, it become an additional unknown of the problem. The resolution principle is as follows. First, a planet gear is defined as reference. Contact points for the other gears are deduced for each successive angular position θ of the reference gear. With knowledge of the contact line location between the sun and the planets, the contacts between ring and planets are deduced from geometrical construction. The resolution of contact equations of each mesh j is:

$$\begin{cases} \mathbf{H_j P_j} = \delta_j(\theta).\mathbf{1} - \mathbf{e_j} \\ \mathbf{P_j} = F_j \end{cases} \tag{1}$$

At each contact, the constraints are:

$$\begin{cases} -\mathbf{H_j P_j} + \delta_j(\theta).\mathbf{1} \leq \mathbf{e_j} \\ \mathbf{P_j} \geq 0 \end{cases} \tag{2}$$

With:

- $\mathbf{H}$ the compliance matrix,
- $\mathbf{P_j}$ the vector of the load distribution on the contact line,
- $\delta_j(\theta)$ the STE at mesh j, which corresponds to a linear displacement of the gear related to the pinion along the line of action,
- $\mathbf{e_j}$ the vector of the initial gaps between the contact surfaces determined from tooth modifications and manufacturing errors,
- F_j the static load oriented along the line of action, induced by the input torque,
- $\mathbf{1}$ a unitary vector used for dimensional considerations.

Furthermore, the instantaneous local mesh stiffness is defined from the derivative of the force transmitted by the mesh in relation to the static transmission error, for each angular position of the driving gear and for each mesh:

$$k_j(\theta_s) = \frac{\partial F_j}{\partial \delta_j}(\theta_s) \tag{3}$$

3.2 Dynamic response of the kinematic chain by a spectral iterative method

The numerical model proposed is based on the following main assumptions:

- The ring gear is assumed to be axisymmetric. Thus, the modal basis is independent of the angular position of the planets. As a result, one modal basis is enough to solve equations at each angular position.
- The equations of motion are first solved in a reference frame associated with the carrier, which is equivalent to considering that the ring gear is moving in this reference frame. This lead to the modal basis being computed in this frame. Indeed, the maximum relative speed of the ring gear to the carrier is about 12 m/s. This represents about 0.2% of the pressure wave propagation speed of 5200 rpm.
- Gyroscopic and centrifugal effects are neglected, as the carrier rotational speed is low in this application.

To access the modal behavior of the gearbox, a 3D finite element model is built, see Figure 3. The housing, gears, input and output shafts and the carrier are modelled using 3D elements. The bearings are modelled using axial and radial spring elements. Inertias are used to model the presence of a motor and a brake. These boundary inertias are connected to the input and output shafts with torsional stiffnesses, modelling the flexible couplings on the test bench. Mean mesh stiffness values are included in the finite element model to ensure kinematic links between the gears.

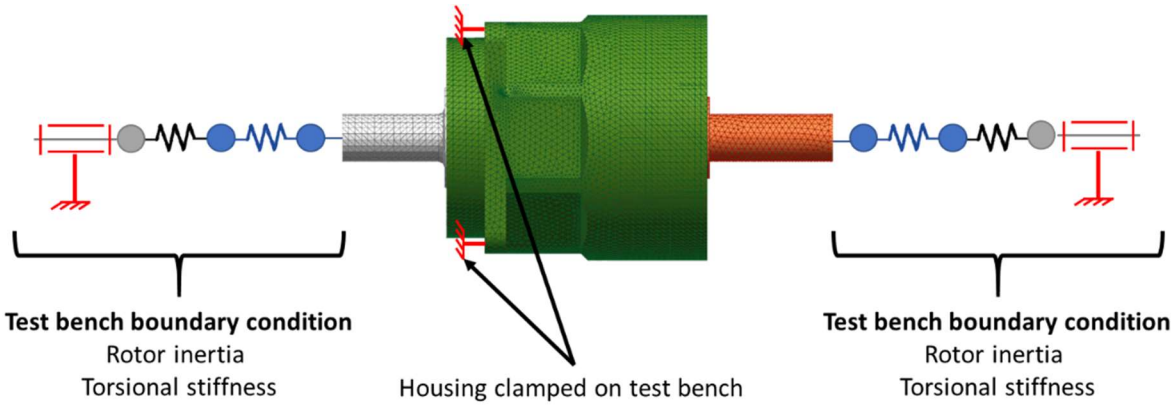

Figure 3: Finite element model of the planetary gear

The equations of motion are expressed from the linearized teeth dynamic loads:

$$\mathbf{M_{EF}}\ddot{x} + \mathbf{C}\dot{\mathbf{x}} + \mathbf{K_{EF}}x + \sum_{j=1}^{m} k_j(t)\,\mathbf{R_j}\mathbf{R_j^T}\mathbf{x} = \sum_{j=1}^{m} k_j(t)\,\mathbf{R_j}\mathbf{R_j^T}\mathbf{x_s}(t) \qquad (4)$$

With $\mathbf{M_{EF}}$ and $\mathbf{K_{EF}}$ respectively the mass and stiffness matrix from the finite element model and $\mathbf{C}$ the damping matrix considered a posteriori through the Basile hypothesis. R_j is the structural vector that couples the wheel, $R_j^T x$ is the dynamic transmission error and $R_j^T x_s$ the static transmission error.

Time discretization methods lead to prohibitive calculation times, as low frequencies require long time periods and high frequencies require fine time sampling. Hence, parametric equations of motion are solved using the spectral iterative method, where large systems of periodic differential equations can be solved with minimal calculation times. The method is detailed in [7]. Previous studies have demonstrated the validity of this method for multi-meshing systems [4], like planetary gear sets [8].

3.3 Vibroacoustic response of the planetary gear housing

The dynamic response computation with the spectral iterative method makes it possible to describe the vibratory state of any point of the finite element model. However, at this step the dynamic resolution is performed neglecting the relative mobility of the planets regarding the ring gear. Thus, no modulation effects can be observed. In order to introduce the effects of

modulation due to carrier rotation at its rotational frequency [9], a complementary computational step is needed to compute the response of any point on the ring gear. The principle is based on a change of reference frame, by considering the effect induced by the relative rotation between the observation point (fixed point located on the ring gear) and the meshes (attached to the carrier reference frame).

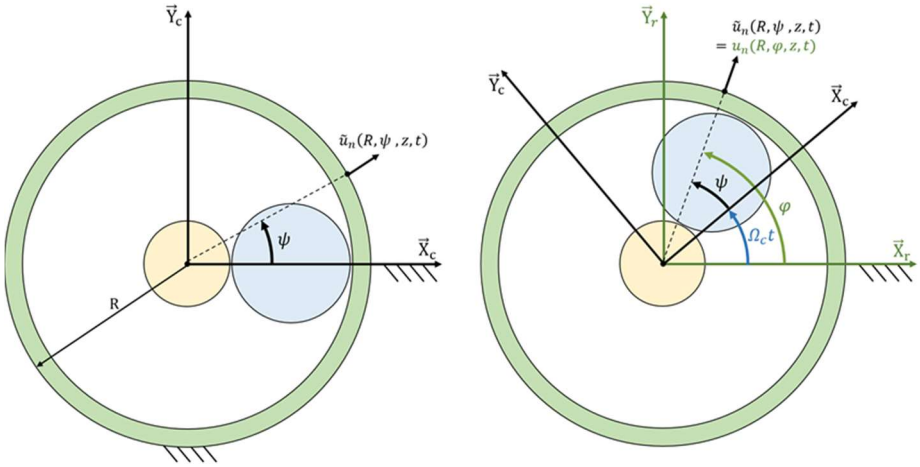

Figure 4: Ring gear dynamic response computation – Numerical model.

The radial dynamic response of the cylindrical ring gear node #n is noted $\tilde{u}_n(R,\psi,z,t)$. The angular position of the observation point is noted ψ and in the carrier reference frame $(\vec{X}_c,\vec{Y}_c,\vec{Z}_c)$ and φ in the housing frame $(\vec{X}_r,\vec{Y}_r,\vec{Z}_r)$. The dynamic responses are computed by considering the system under torque, without any relative movement between the ring gear and the carrier. Figure 4 depicts the different terms introduced. In practice, the dynamic response $u_n(R,\varphi,z,t)$ of a fixed point on the ring gear (in relative motion to the carrier) is measured.

By choosing the initial position of the carrier at $t = 0$, one can write:

$$u_n(R,\ \varphi,\ z,\ t) = \tilde{u}_n(R,\ \psi,\ z,\ t) = \tilde{u}_n(R,\varphi - \Omega_c t,z,\ t) \tag{5}$$

Therefore, a point $B(R,\varphi_B,z_B,t)$ on the ring gear has a dynamic response out of phase from point $A(R,\varphi_A,z_A = z_B,t)$, with a delay of:

$$t_B - t_A = -\frac{\varphi_B - \varphi_A}{\Omega_c} \tag{6}$$

With Ω_c the planet carrier rotational speed. This lead leads to:

$$u_n(R,\ \varphi_B,\ z_B,\ t) = u_n\left(R,\ \varphi_A,\ z_A = z_B,\ t - \frac{\varphi_B - \varphi_A}{\Omega_c}\right) \tag{7}$$

To access the dynamic response $u_n(R,\ \varphi_n\ ,\ z,\ t)$, a linear temporal interpolation between the responses $\tilde{u}_i(R,\ \psi_i,\ z,\ t)$ is built. This interpolation is based on the assumptions of axisymmetry of the ring gear and invariability of the modal basis whatever the position of the planet axis.

On the time interval $t_i \le t \le t_{i+1}$, the following linear time interpolation scheme is proposed:

$$\begin{aligned} &u_n(R,\ \varphi_i,\ z,\ t) \\ &= \frac{\tilde{u}_n(R,\ \varphi - \Omega_c t_i,\ z,\ t)(t_{i+1} - t) + \tilde{u}_n(R,\ \varphi - \Omega_c t_{i+1},\ z,\ t)(t - t_i)}{(t_{i+1} - t)} \end{aligned} \tag{8}$$

From a practical point a view, the iterative spectral method gives access to the answers in discrete nodes i of the ring gear $\tilde{u}_i(R,\ \psi_i, z,\ t)$, $i = 1$ to G (54 points considered in our application).

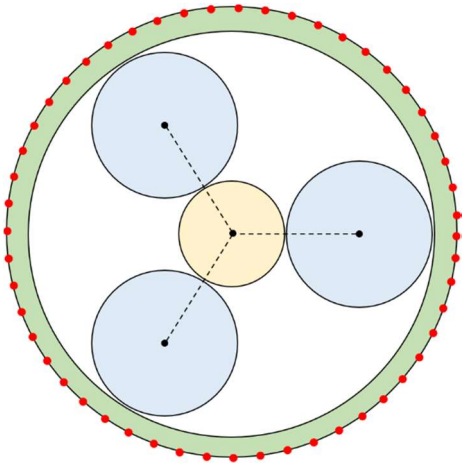

Figure 5: Localization of the 54 nodes along the ring gear.

Considering discretization of the ring gear, the answer $u_n(R,\ \varphi,\ z,\ t)$ is evaluated at the node of the model identified by:

$$\varphi_k = \frac{2k\pi}{G}, (k = 0, 1, \dots G-1) \tag{9}$$

i.e. $u_n(R,\ \varphi_k,\ z,\ t)$. From equation 8 ones obtains:

$$u_n(R,\ \varphi_k,\ z,\ t) = \frac{\tilde{u}_n(R,\ \varphi_k - \Omega_c t_i,\ z,\ t)(t_{i+1} - t) + \tilde{u}_n(R,\ \varphi_k - \Omega_c t_{i+1},\ z,\ t)(t - t_i)}{(t_{i+1} - t)} \tag{10}$$

Where t_i is chosen such that:

$$t_i = \frac{2i\pi}{G\Omega_c}, i \in \mathbb{N} \tag{11}$$

Thus, the time interval becomes:

$$t_{i+1} - t = \frac{2\pi}{G\Omega_c} \tag{12}$$

Finally, the dynamics response of the nodes identified by the angle φ_k at time t is equal to:

$$u_n(R,\ \varphi_k,\ z,\ t) = \frac{G\Omega_c}{2\pi}\sum_{i=0}^{G-1}\left[\tilde{u}_i\left(R, \frac{2\pi(k-i)}{G},\ z,\ t\right)(t_{i+1} - t) + \tilde{u}_i\left(R, \frac{2\pi(k-1-i)}{G},\ z,\ t\right)(t - t_i)\right] H(t - t_{i+1})\, H(t_i - t) \tag{13}$$

For the interval $0 \le t \le T_c$, with H the Heaviside Function.

All the nodes on a peripheral circle of the ring gear have an identical response to within one phase. Therefore, it is sufficient to calculate the response for $\varphi_k = 0$, i.e.

$$u_n(R,\ 0,\ z,\ t) = \frac{G\Omega_c}{2\pi}\sum_{i=0}^{G-1}\left[\tilde{u}_n\left(R,\frac{2\pi(G-i)}{G},\ z,\ t\right)(t_{i+1}-t)\right. \\ \left. + \tilde{u}_n\left(R,\frac{2\pi(G-1-i)}{G},\ z,\ t\right)(t-t_i)\right]H(t-t_{i+1})\,H(t_i-t) \tag{14}$$

4. NUMERICAL RESULTS

Two test cases are discussed:

- Dynamic response at a low speed (250 rpm), when the harmonics of the mesh frequency are lower than the system's eigenfrequencies,
- Dynamic response at a high speed (3100 rpm), when the harmonics of the mesh frequency may coincide with frequencies for which the ring gear exhibits significant operational dynamic deformation.

4.1 Dynamic response of the ring gear at a low speed

The dynamic response of the ring gear is evaluated for a sun gear rotational speed of 250 rpm. The mesh frequency is then equal to $f_m = 90$ Hz. At low rotational speeds, the first harmonics of the mesh frequency are lower than the first natural mode of the system, thus the ring gear responds on its static deformation, i.e. the static contribution of the modes. This static deformation, calculated by considering unitary forces directed along the lines of action, is shown in Figure 6.

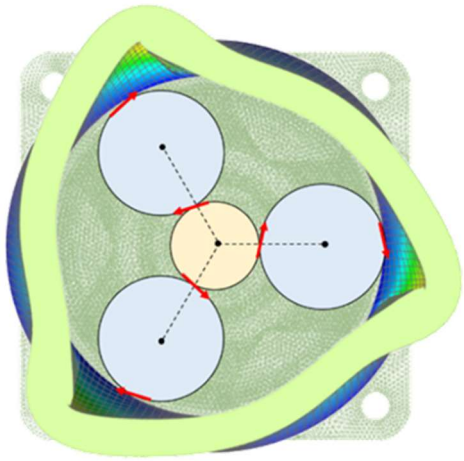

Figure 6: Static deformation of the ring gear induced by unitary force oriented along the line of action.

Figure 7 (a) depicts the time evolution of the dynamic response of the ring gear for one carrier rotational period T_c, for purely harmonic excitation at the mesh frequency H_{108}, and Figure 7 (b) its associated spectrum, plotted as a function of the planet carrier order.

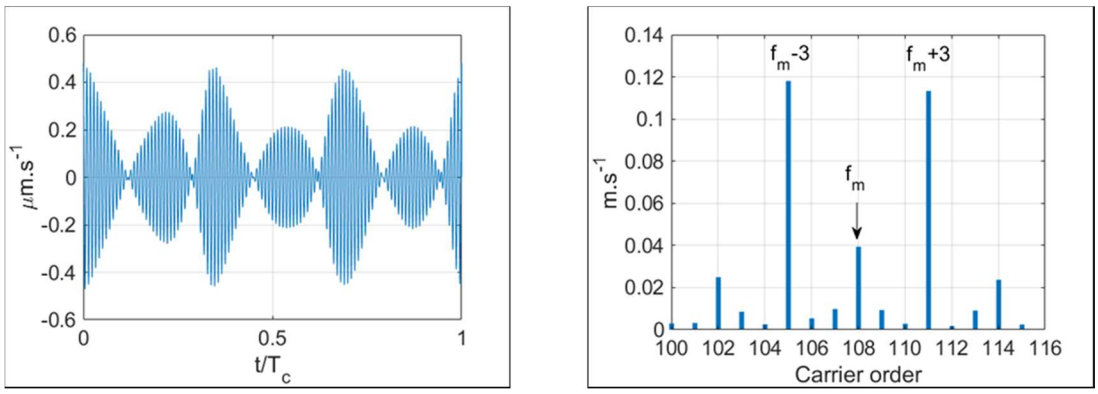

(a) (b)

Figure 7**:** (a) Temporal evolution of the ring gear dynamic response at 250 rpm. (b) Amplitude spectra in function of the mesh frequency order.

A perfectly axisymmetric finite element model would present a periodic temporal response with a period equal to $T_c/3$, corresponding to the periodic passage of the three planets. In the current application, there is a slightly different behavior because the system is not perfectly axisymmetric. It is also clear that the envelope of the temporal response has six lobes, reflecting the amplitude modulation phenomena. The spectrum has a moderate amplitude at the mesh frequency f_m. The dominant lines are the sidebands at $f_m \pm N$, where N is the number of planets. Detailed analysis of the time response envelope for this operating regime makes it possible to establish a link between its amplitude and the static deformation of the ring gear (see Figure 6).

4.2 Dynamic response of the ring gear at high speed

For high operating regimes, the mesh frequency harmonics are high enough to coincide with the system's eigenmodes. To illustrate the impact of this coincidence, the dynamic response of the ring gear is considered for a sun rotation speed equal to 3100 rpm. The mesh frequency is then equal to 1116 Hz.

Figure 8(a) shows the time evolution of the modulated dynamic response of the ring gear. Figure 8(d) the amplitude spectrum, plotted as a function of the carrier frequency order. An amplification of the fifth and sixth harmonics of the mesh frequency is observed, corresponding to an excitation of the modes around 5 580 and 6 695 Hz. A detailed analysis of the contribution of these two harmonics, depicted in Figures 8(b) and (c) (temporal evolution) and Figures 8(e) and (f) (amplitude spectrum), highlights that the amplitudes of the mesh frequency harmonics H_{540} and H_{648} are lower than that of the sidebands at $H_{108}\times i \pm N H_1$ and $H_{108}\times i \pm k H_1$, with N the number of planets and k an integer. The shape of the temporal dynamic responses' envelope is complex and depends on the frequency of observation, and thus on the modes exited. The number of lobes seems to be driven by the difference between the two most significant sidebands. For example, there are six lobes for the dynamic response around the fifth harmonic (driven by the sidebands H_{537} and H_{543}), while there are four lobes for the dynamic response around the sixth harmonic (driven by the sidebands H_{645} and H_{649}). The global dynamic time response results from the superposition of the different dynamic responses extracted around the mesh frequency harmonics.

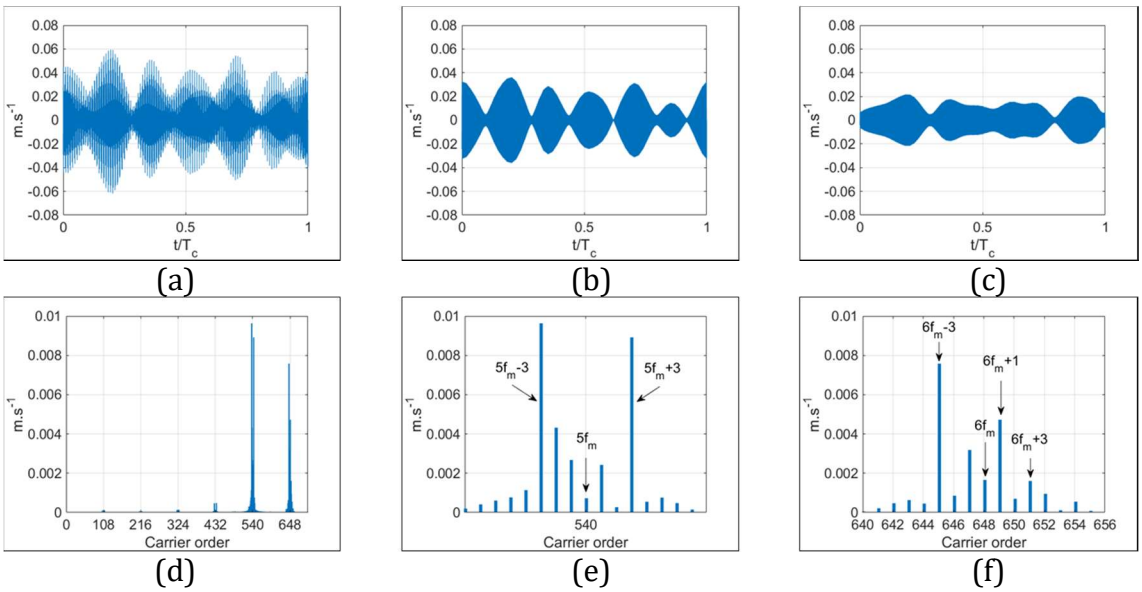

Figure 8: (a) Temporal evolution of the overall ring gear dynamic response at 3100 rpm. (b) Temporal evolution of the ring gear dynamic response on the order range [532 548]. (c) Temporal evolution of the ring gear dynamic response on the order range [640 656]. (d) Amplitude spectra of the overall ring gear dynamic response. (e) Amplitude spectra of the ring gear dynamic response on the order range [532 548]. (f) Amplitude spectra of the ring gear dynamic response on the order range [640 656].

4.3 Dynamic response of the ring gear – experimental point of view

This section presents the verification of the consistency of the numerical observations with the actual behavior of the planetary gear. For the comparison between computation and measurement, the dynamic responses are extracted around the first four harmonics of the mesh frequency, including sidebands induced by carrier rotation.

The experimental dynamic response measured at 800 and at 2 200 rpm is presented in Figure 9 (a, b) by retaining only the frequency contributions on the order band $H_{108}\times i\pm N H_1$, (i=1, 2… 6), N being the number of planets. A signal with a complex modulation is observed, where it is difficult to observe the three planets passing in front of the sensor. As for the numerical analysis, Figure 9 (c, d) shows the vibratory level extracted from specific mesh harmonic orders. The dynamic response at 800 rpm shows 5 lobes, whereas at 2 200, 6 lobes are observed. The experimental observations are qualitatively consistent with what is observed numerically, and highlight the modelling limitations that neglect gearbox modal behavior.

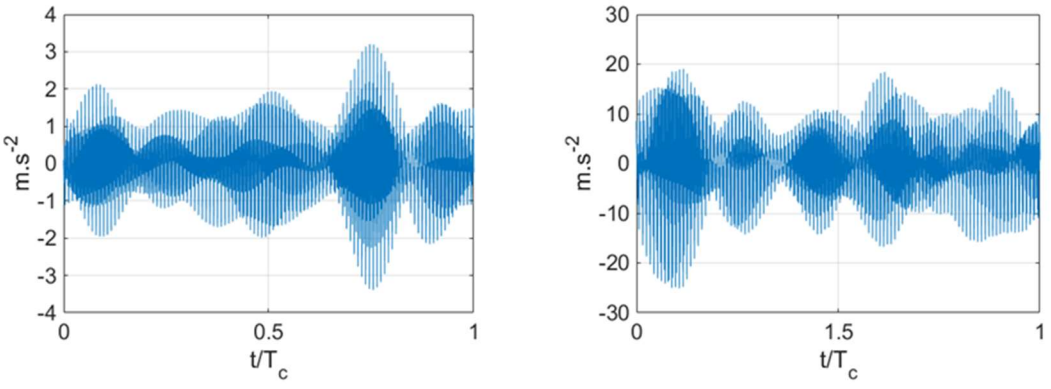

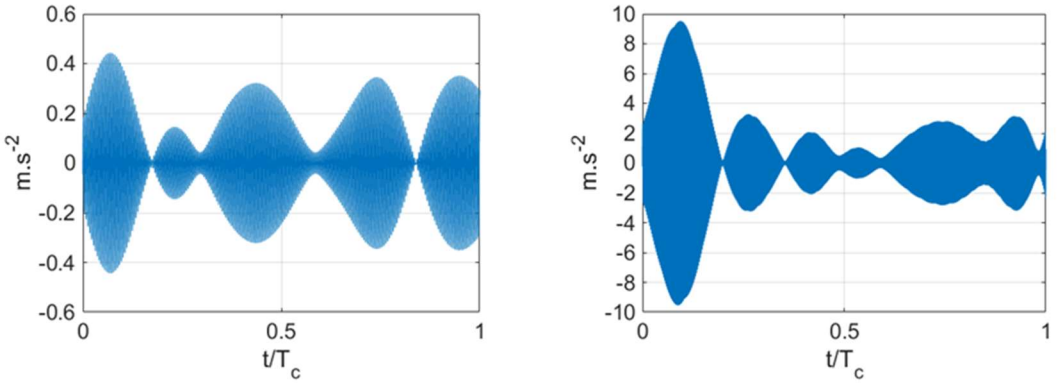

(c) (d)

Figure 9: (a) Ring gear dynamic response measured at 800 rpm. (b) Ring gear dynamic response measured at 2200 rpm. (c) Ring gear dynamic response measured at 800 rpm, order 2 of the mesh frequency. (d) Ring gear dynamic response measured at 2200 rpm, order 4 of the mesh frequency

5. CONCLUSION

The modulated dynamic response of the planetary gear's ring gear is evaluated using an original approach which considers its operational deformation for each operating regime. The numerical results show that for low sun rotational speeds, the envelope of the ring gear's dynamic response is driven by the static deformation of the planetary gear. At higher rotational speeds, when the harmonics of the mesh frequency are high enough to coincide with the system's eigenmodes, the envelope of the modulated dynamic response is driven by the ring gear's operational deformation. Measurement investigations show that the modulations of the ring gear's dynamic response can present more lobes than the number of planets; results of a complex behavior.

The use of the spectral iterative method offers low computational time and gives the opportunity to extract the dynamic response at several points to construct a refine modulated response. It also offers the opportunity to perform parametrical simulation, the key to a better understanding of ring gear modulation dynamic response effects.

ACKNOWLEDGEMENTS

This work has been performed within the LabCom LADAGE (Laboratoire de dynamique des engrenages) funded by the French National Research Agency / ANR under the reference number ANR-14-LAB6-0003, a partnership between Vibratec and the LTDS.

REFERENCES

[1] DB. Welbourn, Fundamental knowledge of gear noise – a survey. Proc Conf Noise Vibrat Engines Trans 1979; C177/79: 9–29.

[2] SL. Harris, Dynamic loads on the teeth of spur gears. Proc IMechE 1958; 172: 87–112.

[3] E. Rigaud, J. Sabot, Effect of elasticity of shafts, bearings, casing and couplings on the critical rotational speeds of a gearbox. VDI Berichte 1996; 1230: 833–845.

[4] A. Carbonelli, E. Rigaud, J. Perret-Liaudet, Vibro-acoustic analysis of geared systems – predicting and controlling the whining noise. Automotive NVH Technology, Fuchs A, Nijman E and Priebsch H-H (Eds), Springer briefs in applied sciences and technology. Springer International Publishing 2016, pp.63–79.

[5] P.D. MacFadden and J.D. Smith, An explanation for the asymmetry of the modulation sidebands about the tooth meshing frequency in epicyclic gear vibration, Proceeding of the Institution of Mechanical Engineers, Part C : Journal of Mechanical Engineering Science, vol.199, no 1, pp. 163-172, 1991

[6] J. McNames, Fourier serie Analysis of Epicyclic Gearboc Vibration, Journal of Vibration and Acoustics, vol. 124, no. 1, pp 150-153, 2002
[7] J. Perret-Liaudet, “An original method for computing the response of a parametrically excitated forced system,” JSV, vol. 196, 1996, 165-177.
[8] J.Neufond, E. Denimal, E. Rigaud, J.Perret-Liaudet, A.Carbonelli, Whining noise computation of a planetary gear set induced by the multi-mesh excitations. Proc. Inst. Mech. Eng. C, 2019
[9] M. Inapolat and A. Kahraman, A theoretical and experimental investigation of modulation sidebands of planetary gear sets, Journal of Sound and Vibration, vol. 323, no 3-5, pp. 677-696, 2009.
[10] D. Ploger, ¨ C. Fischer, S. Rinderknecht, Linking the modulation of gear mesh vibration in planetary gearboxes to manufacturing deviations, Mech. Syst. Signal Process 155 (2021), 107554.
[11] K. Morikawa, K. Kumagai and R. Nishihara, A study on the sideband phenomenon of planetary gears, Transaction of the JSME (in Japanese), vol. 80, no. 815, 2014